Seasonal sea ice prediction based on regional indices

John E. Walsh[1], J. Scott Stewart[2], Florence Fetterer[2]

[1]Alaska Center for Climate Assessment and Policy, University of Alaska, Fairbanks, AK 99709 USA
[2]National Snow and Ice Data Center, University of Colorado, Boulder, CO 80303 USA

Correspondence to: John E. Walsh (jewalsh@alaska.edu)

Abstract. Basic statistical metrics such as autocorrelations and across-region lag correlations of sea ice variations provide benchmarks for the assessments of forecast skill achieved by other methods such as more sophisticated statistical formulations, numerical models, and heuristic approaches. However, the strong negative trend of sea ice coverage in recent decades complicates the evaluation of statistical skill by inflating the correlation of interannual variations of pan-Arctic and regional ice extent. In this study we provide a quantitative evaluation of the contribution of the trend to the predictive skill of monthly and seasonal ice extent on the pan-Arctic and regional scales. We focus on the Beaufort Sea where the Barnett Severity Index provides a metric of historical variations in ice conditions over the summer shipping season. The variance about the trend line differs little among various methods of detrending (piecewise linear, quadratic, cubic, exponential). Application of the piecewise linear trend calculation indicates an acceleration of the trend during the 1990s in most of the Arctic subregions. The Barnett Severity Index as well as September pan-Arctic ice extent show significant statistical predictability out to several seasons when the data include the trend. However, this apparent skill largely vanishes when the data are detrended. No region shows significant correlation with the detrended September pan-Arctic ice extent at lead times greater than a month or two; the concurrent correlations are strongest with the East Siberian Sea. The Beaufort Sea's ice extent as far back as July explains about 20% of the variance of the Barnett Severity Index, which is primarily a September metric. The Chukchi Sea is the only other region showing a significant association with the Barnett Severity Index, although only at a lead time of a month or two.

1 Introduction

One of the most widely monitored variables in the climate system is Arctic sea ice. By any measure, Arctic sea ice has decreased over the past few decades (AMAP, 2017). September sea ice extent during the past 5-10 years has been approximately 50% of the mean for the 1979-2000 period. (Consistent measurements by satellite passive microwave sensors began in 1979). The recent decline is unprecedented in the satellite record, in the period of direct observations dating back to 1850 (Walsh et al., 2016), and in paleo reconstructions spanning more than 1400 years (Kinnard *et al*., 2011). The recent reduction of sea ice has been less in winter and spring than in summer and autumn, resulting in a sea ice cover that is largely seasonal (AMAP, 2017). The increasingly seasonal ice cover contrasts with the Arctic Ocean's predominantly multiyear ice pack of the pre-2000 decades. When compared to the reductions of the spatial extent of sea ice, the percentage reductions of ice volume and thickness are even larger. Ice thickness decreased by more than 50% from 1958-1976 to 2003-2008 (Kwok and Rothrock, 2009), and the percentage of the March ice cover made up of thicker multiyear ice (ice that has survived a summer melt season) decreased from 75% in the mid-1980s to 45% in 2011 (Maslanik *et al*., 2011). Laxon et al. (2013) indicate a decrease of 64% in autumn sea ice volume from 2003-08 to 2012.

While the loss of sea ice is generally presented in terms of pan-Arctic metrics, regional trends can be quite different from the pan-Arctic trends. The Bering Sea, for example, showed a positive trend of coverage (fewer open water days) from 1979 through 2012 (Parkinson, 2014), even though regions to its north (the Chukchi and Beaufort Seas) showed some of the largest decreases of summer ice coverage in the entire Arctic (Onarheim et al., 2018). The other area of strong decreases of ice coverage has been the Barents/Kara Sea region.

The Beaufort Sea serves as an illustrative example of the impacts of trends and variability of sea ice. The number of open water days immediately offshore of the Beaufort coast has been 60-120 in recent years. Parkinson's (2014) Figure 2 shows that the number of open water days increased by 20-30 days per decade over the period 1979-2013. However, as recently as the 1970s, there were summers with little or no open water in this region, as described by Crowley Maritime, one of the major barge operators in the Alaska region:

58   "With pipeline construction well underway in 1975, the Crowley summer sealift

59   flotilla to the North Slope faced the worst Arctic ice conditions of the century. In fleet

60   size, it was the largest sealift in the project's history with 47 vessels amassed to carry

61   154,420 tons of cargo, including 179 modules reaching as tall as nine stories and

62   weighing up to 1,300 tons each. Vessels stood by for nearly two months waiting for the

63   ice to retreat. Finally in late September the ice floe moved back and Crowley's tugs and

64   barges lined up for the slow and arduous haul to Prudhoe Bay. When the ice closed again,

65   it took as many as four tugs to push the barges, one at a time, through the ice".

66   — *From Crowley Maritime, 50 Years of Service in Alaska (2002)*

67   As will be shown, the contrast between present-day ice conditions and the Crowley

68   experience of the 1970s is largely a manifestation of the trend of Beaufort Sea ice cover.

69   However, sea ice also exhibits large year-to-year variability, which has been superimposed on

70   the recent trend towards less sea ice in the Arctic. This variability challenges users of coastal

71   waters in various sectors and lies at the heart of the sea ice prediction problem. While the

72   climatological seasonal cycle and even observed trends provide an initial expectation for the sea

73   ice conditions that will be present in a particular region at a particular time of year, the

74   departures from the climatological mean, whether or not the mean is adjusted for a trend, is

75   affected by the atmospheric forcing (winds, air temperatures, radiative fluxes) and oceanic

76   forcing (currents, water temperatures) of the particular year. These departures have a large

77   component of internal variability and hence are difficult to predict over monthly and seasonal

78   timescales (Serreze et al., 2017), raising questions about the extent to which sea ice variations

79   may be predictable. Even ice-ocean models, which are initialized to current sea ice and ocean

80   conditions, require atmospheric and oceanic forcing in order to predict future ocean states. The

81   predictability of sea ice variations beyond the mean seasonal cycle and ongoing trends is the

82   main focus of this paper.

83   The present paper also extends Drobot's (2003) study of the predictability of Beaufort-

84   Chukchi sea ice. Drobot used data from 1979-2000 to assess predictability of a measure of

85   Beaufort Sea summer ice severity (Section 2 below) based on antecedent sea ice conditions as

86   well as several atmospheric indices. While some skill was found in predictions based on

87   indicators from the previous seasons, the limited sample of years used in developing the

88   statistical models raises questions about broader applicability. In this regard, Drobot (2003, p.

89   1161) states "…if the Arctic climate changes, the methods described here will need to be

90   altered". In fact, the Arctic climate and, in particular, its sea ice regime, have changed with the

91   unprecedented retreat of sea ice in the post-2000 period. The impact of the trend on statistical

92   predictability is a focus of the present paper. Another relevant study is that of Blanchard-

93   Wrigglesworth et al. (2011), who found evidence that persistence of ocean temperature

94   anomalies across seasons has a detectable impact on sea ice variations, implying some

95   predictability over seasonal timescales. However, as with Drobot (2003), the extent to which

96   such relationships are affected by detrending remains to be established.

97   The present paper has three main objectives: (1) to quantify predictability inherent in

98   antecedent spatial distributions of sea ice, (2) to distinguish predictability of pan-Arctic sea ice

99   from that of regional predictability, and (3) to distinguish quantitatively the trend-derived

100   predictability and predictability of departures from trend.

101   More generally, the results presented here can serve to provide a baseline for distinguishing

102   contributions to sea ice forecast skill arising from seasonal climatologies, persistence, and trend.

103   This baseline can, in turn, serve as benchmarks for measuring improvements achieved by more

104   sophisticated prediction approaches such as ice-ocean models, analog systems, neural networks

105   and other more comprehensive statistical methods. The Sea Ice Prediction Network, previously

106   known as the Sea Ice Outlook (Stroeve et al., 2014), provides an annual compilation of seasonal

107   sea ice forecasts, which are grouped into three categories: physical/dynamical models, statistical

108   methods, and heuristic approaches. While the methodology used in this paper falls into the

109   statistical category, the distinctions between (a) pan-Arctic and regional skill and (b) trend-

110   derived and interannual forecast skill are relevant to all three approaches to sea ice prediction.

2 Metrics of sea ice coverage

112   Historical variations of sea ice are documented using various metrics, including sea ice extent,

113   ice-covered area, and thickness. Sea ice extent is the total area within the ice edge, which is

114   typically taken to be the 15% contour of sea ice concentration. Ice extent is readily obtainable

115   from satellite measurements, as is the actual ice-covered area if the open water within the ice edge

116   is accurately depicted. Surface-based observations from ships or coastal locations typically

117   capture only the ice edge and are therefore useful primarily in the mapping of ice extent. While

118   maps of ice extent exist back to the 1800s, there are no such historical products for ice thickness.

119   *In situ* measurements of ice thickness are sparse in space and time, as are submarine sonar

120   measurements, which are not only sparse but often remain classified. Satellite-derived estimates

121   of ice thickness are subject to considerable uncertainty and have only recently come into use (e.g.,

122   CryoSat), while dynamic-thermodynamic model-based reconstructions of historical sea ice

123   thickness variations have only recently been attempted (Schweiger et al., 2018).

124   To explore predictability that may be inherent in the spatial distribution of sea ice, we compute

125   ice extent using a gridded Arctic-wide sea ice concentration product developed for research

126   applications such as serving as a surface boundary layer in atmospheric studies, or for

127   incorporation in reanalyses. *Gridded Monthly Sea Ice Extent and Concentration, 1850 Onward*

128   (Walsh et al., 2015), referred to in the National Snow and Ice Data Center (NSIDC) catalog as

129   G10010, is based on observations from approximately 15 historical sources between 1850 and

130   1978: the earliest are whaling records, and the most complete, in terms of coverage, are the Arctic-

131   wide analyses that the U.S. Navy complied beginning in the 1950s. Beginning in 1979, sea ice

132   concentrations from passive microwave data are used exclusively in G10010. Ice concentration

133   fields on the 15th of each month are taken from the *NOAA/NSIDC Climate Data Record of Passive*

134   *Microwave Sea Ice Concentration, Version 2 (Meier et al., 2013).*

135   Prior to the 1950s, most observations were from near or just within the ice edge. If only the

136   ice edge position was known, a gradient of ice concentration within the edge was imposed in order

137   to integrate the observations into G10010. The gradient was based on a climatology constructed

138   from the passive microwave data. Spatial and temporal gaps in observations were filled using an

139   analog technique that is described in the data product documentation. Each month's sea ice

140   concentration field in G10010 is an estimate of conditions at one time in the month, nominally the

141   15th day of the month (or as close to the 15th as data were available). The fields are at quarter-

142   degree resolution. From these fields one can derive monthly sea ice extent values. Sea ice extent

143   is computed as the area, in sq km, covered by all cells that contain ice in any concentration greater

144   than 15%. Sea ice extent is always greater than or equal to the actual ice-covered area, which

145   excludes the area of open water within the main ice pack.

146   Various studies (e.g. Partington et al., 2003; Agnew and Howell 2002) have shown that

147   passive microwave-derived sea ice data tend to underestimate ice concentration when compared

148   with operational analyses. The *Climate Data Record of Passive Microwave Sea Ice Concentration*

149 is a blend of output from two algorithms that results in higher ice concentrations overall for a better

150 match with the operational analyses that predate the satellite record. Even so, one might expect

151 to see a discontinuity in the G10010 time series of ice extent when the passive microwave record

152 starts in 1979, but this is not evident (see Fig. 10 in Walsh et al., 2016). While G10010 gives a

153 record of ice extent that has realistic variability back to 1850, it is difficult to assign an uncertainty

154 to the concentration fields and ice extent values derived from them. Ice extent will be more

155 accurate than actual ice-covered area because there are many more observations of the ice edge

156 than of the concentrations within interior pack. For this reason, we base our analysis on ice extent.

157   G10010 was used to compute the time series of monthly sea ice extent for the pan-Arctic

158 domain and various Arctic subregions in which sea ice is at least a seasonal feature. The

159 regionalization adopted here follows that of the MASIE (Multisensor Analyzed Sea Ice Extent)

160 product available from the National Snow and Ice Data Center

161 (http://nsidc.org/data/masie/browse_regions). MASIE is produced in cooperation with the U.S.

162 National Ice Center (NIC), and its regions are defined on the basis of NIC operational analyses

163 areas. We use the following MASIE regions: (1) Beaufort Sea, (2) Chukchi Sea, (3) East Siberian

164 Sea, (4) Laptev Sea, (5) Kara Sea, (6) Barents Sea, (7) East Greenland Sea, (8) Baffin Bay/Davis

165 Strait, (9) Canadian Archipelago, (10) Hudson Bay, (11) central Arctic Ocean and (12) Bering Sea.

166 There are several other MASIE regions (Baltic Sea, Yellow Sea, Cook Inlet) that are not used here

167 because they are not geographically connected with the main Arctic sea ice cover. Figure 1 shows

168 the regions.

169   We also make use of the long ice extent record provided by G10010 to investigate the

170 predictability of the Barnett Severity Index, or BSI. The BSI is directly relevant to offshore

171 navigation applications in the Beaufort Sea. It is a metric of the severity of ice conditions, such as

172 conditions encountered by barges resupplying the North Slope. The BSI is determined once per

173 year, at the end of the summer shipping season, by analysts at the U.S. National Ice Center. It is a

174 unit-less linear combination of five parameters: 1) the distance in nautical miles from Point Barrow

175 northward to the ice edge on 15 September, 2) the distance from Point Barrow northward to the

176 4/8th ice concentration line on 15 September, 3) the number of days the entire sea route from the

177 Bering Strait to Prudhoe Bay is ice-free in a calendar year, 4) the number of days the entire sea

178 route to Prudhoe Bay is less than or equal to 4/8th ice concentration in a calendar year, and 5) the

179 temporal length of the navigable season, defined as the time period from the initial date the sea

180   route is less than 4/8th ice concentration to 1 October (Barnett, 1980). Figure 2 is a time series of

181   the BSI reconstructed from gridded sea ice concentration data (see Appendix). Higher values

182   indicate less severe ice conditions.

3 Methods

184   As shown in Figure 3, Arctic sea ice extents have generally been decreasing. The Beaufort

185   Sea is a prime example of a region in which summer and autumn sea ice coverage has been

186   decreasing, although winter (March) sea ice extent in the Beaufort Sea shows no trend or variability

187   because the ice edge extends to the coastline in March of every year, essentially eliminating year-

188   to-year variations. Consistent with the September decrease of Beaufort ice extent, the BSI has been

189   increasing over the past few decades. Two time series containing trends over time can show a

190   correlation simply because the trends are present in the time series. A trend can be used as a

191   predictive tool by assuming its continuation into the future. However, continuation of a trend and

192   anticipation of it can inflate forecast skill in predictions of interannual variations. Indeed,

193   depictions of time-variations of a quantity such as sea ice extent are often shown as departures

194   from a trend line in order to highlight the interannual variations. Because one of our main interests

195   in this study is whether or not interannual variations of preceding regional extent values correlate

196   with later BSI values, so want to exclude the effect of the overall trends in the correlation of these

197   time series. To do this, we must de-trend the data in the time series.

198   The choice of a function with which to de-trend the time series should be determined by

199   features of the series itself. The detrended time series should exclude the general tendency to

200   change over time, but preserve a measure of the year-to-year variability of the series. Because the

201   change in sea ice extent is more pronounced in the most recent decades (Figure 3), it is not

202   sufficient to simply detrend using a multi-decadal linear fit to the time series.

203   We explored several functional forms which fit the time series, including linear, quadratic,

204   cubic, and exponential functions. We found that a simple two-piece linear function – wherein the

205   data are modeled by two line segments that intersect at a 'break-point' year – had the lowest

206   average RMS difference between the time series and the fitted function, although fits using other

207   functions had only slightly larger RMS differences. This choice of the detrending fit has the

208   additional feature of giving a sense of when the ice extent trend began to change more strongly.

209   The two-piece linear fits were obtained by using standard statistical algorithms. A function

210   defined by two intersecting half-lines can be specified by the coordinates of one point on each

211   half-line and the intersection point. With the x-axis as time, and the y-axis as the value of the sea

212   ice extent, the x-values of the non-intersecting points can be chosen to be 1953 and 2013, the first

213   and last years of the BSI dataset. This leaves four values for the function to fit: the series value in

214   1953, the series value in 2013, and the year and value at the intersection point, also referred to here

215   as the break-point. We note that the break-point is not specified by the user but is determined by

216   the algorithm so that the fit to the time series is optimized.

217   The two-piece linear fit was generated by allowing the SciPy 'curve_fit' routine (Jones et al.,

218   2001) to iterate to a solution. The 'curve-fit' method in the SciPy programming library permits

219   users to define an arbitrary function and to find a minimal least squares fit of that function's

220   coefficients to a given dataset. The two-piece linear fit was used to detrend the BSI values as well

221   as the time series of the regional and pan-Arctic ice extents. In Figure 4, we show these various

222   fits to the time series of the BSI and the September Beaufort Sea ice extent. In the case of the two-

223   piece linear fit, the break-point (chosen to minimize the departures from trend) is in the early

224   1990s. It is visually apparent from Figure 4 that all four fits are comparable in terms of the overall

225   magnitudes of the departures from the trend lines. The root-mean-square departures from the

226   various trend lines indeed differed by less than 10%. Given the small differences between the fits,

227   we choose the two-piece linear for for the remainder of this study. An additional reason for

228   selecting the two-piece linear fit is that it allows comparisons of the timing of the break-points

229   across the various subregions.

230   After using the 'linregress' method from the SciPy (Jones et al., 2001) software library to fit

231   a line to regional monthly extent values and the BSI, we computed correlations between the

232   departures of the two time series from their respective two-piece trend lines. For comparison, we

233   also computed correlations between the "raw" (with trends) time series. The square of the Pearson

234   correlation coefficient (R^2) was computed using the 'stats' method from the SciPy package and

235   was used to determine whether and how strongly the two time-series are correlated with each other.

236

237   **4 Results**

238

239   Because changes of trend have not been addressed systematically in previous evaluations of

240   Arctic sea ice trends, we synthesized the break-point information across all regions and calendar

241   months (January-September) included in our study. Figure 5 groups the break-points into five year

242   periods ending in 1955, 1960,…, 2015. Nearly all the break-points occur in the second half of the

243   study period, with a maximum in 1991-1995. The 1991-1995 period has more than twice as many

244   break-points as any other 5-year period. The break-points for our focal metrics, the BSI and

245   September pan-Arctic ice extent, are 1991 and 1996, respectively, consistent with the distribution

246   in Figure 5. These two metrics are included in the results summarized in Figure 5. One may

247   conclude that the 1990s, and to a lesser extent the first decade of the 2000s, represent the shift to

248   a more rapid rate of sea ice loss. If one is to argue for a "regime shift" in Arctic sea ice loss

249   (Lenton, 2012), this period would be the leading candidate.

250   In order to illustrate the effect of the detrending, Figure 6 shows the squares of the correlations

251   (R^2) between September pan-Arctic ice extent and the concurrent ice extent in each of the

252   subregions. The R^2 metric is used rather than R because R^2 corresponds to the explained variance.

253   The figure shows values of R^2 before detrending (upper numbers, regular font) and after detrending

254   (lower numbers, bold font). With the trend included, the R^2 values are relatively high in most

255   regions (except for the Bering Sea), ranging from 0.32 to 0.71, corresponding to accrual

256   correlations (R) ranging from 0.57 to 0.84. These correlations all exceed the 95% significance

257   thresholds, which range from 0.26 ($R^2 = 0.07$) for a 60-year samples with no autocorrelation to

258   0.38 ($R^2 = 0.14$) for a 60-year samples with an autocorrelation of 0.4. Because these correlations

259   are dominated by the trend, the larger values appear in the regions with trends that are most similar

260   to the pan-Arctic trend. When the data are detrended, the correlations are much smaller (R^2 values

261   in bold font in Fig. 6) although still larger than the 95% significance thresholds for 60-year samples

262   ($R = 0.26$, $R^2 = 0.07$). These smaller values indicate the relative contributions of regional variations

263   to the interannual variations of pan-Arctic ice extent. According to Figure 6, the regions

264   contributing most strongly to September pan-Arctic variations are the Beaufort and East Siberian

265   Seas.

266   Figure 7 shows the squares of the correlations between the annual BSI and regional

267   September ice extent before detrending both ice extent and the BSI (top number) and after

268   detrending (bottom number). While the actual correlations between the BSI and regional extent

269   are generally negative, the R^2 values plotted in Figure 7 are positive. Large values of R^2 appear in

270   most regions when the trend is included (upper numbers) because the BSI has a strong positive

271   trend over time while September ice extent in most regions has a negative trend. The R^2 values

272   are much weaker in regions away from the Beaufort Sea when the trends are removed (lower

273   numbers in Fig. 7). The detrended R^2 values show the spatial representativeness of the BSI as a

274   measure of interannual variations; this representativeness is limited primarily to the Beaufort and

275   Chukchi Seas, with a weak extension into the East Siberian Sea.

276   Because the potential for seasonal predictions is a key motivation for this study, we

277   examine cross-correlations in which the predictands (pan-Arctic ice extent and the BSI) lag

278   potential predictors (regional ice extents) by intervals ranging from zero (no lag) to several

279   seasons. Cross-correlations between non-detrended and detrended September pan-Arctic and

280   regional ice extent are summarized in Tables 1 and 2 respectively. Cross-correlations between

281   non-detrended and detrended BSI and regional ice extent are given in Tables 3 and 4

282   respectively. In all cases, the numerical values are the R^2 values. In order to illustrate the

283   contribution of the trend to the apparent predictability, we present these correlations graphically

284   for the regions which show the strongest associations with the September predictands. Figure 8

285   shows the R^2 values for cases in which September pan-Arctic ice extent lags by 0, 1, 2,…,8

286   months the ice extent in four subregions: the Beaufort, Chukchi, East Siberian and Barents Seas.

287   The red bars correspond to correlations computed from the data with the trends included. Not

288   surprisingly, the R^2 values are largest at zero lag. The rates at which the correlations decrease

289   with increasing lag vary regionally, reaching zero by 3-4 months for the Chukchi and East

290   Siberian Seas but remaining weakly positive for the Beaufort and Bering Seas back to the

291   preceding winter. The zero-month lag values are quite large for the Beaufort, Chukchi and East

292   Siberian regions, where they exceed $R^2 = 0.7$ (R = 0.84).

293   However, after detrending (using the two-piece linear best fits), most of the apparent

294   predictability is lost. As shown by the blue bars in Figure 8, nearly all the predictability from the

295   Barents and Chukchi Seas vanishes with the detrending, while only small fractions of explained

296   variance remain at non-zero lags when the Beaufort and East Siberian Seas are the predictors. For

297   example, when the regional extent leads by two months (July), the fractions of explained variance

298   are approximately 0.16 and 0.10 (R ~ 0.40 and 0.32) for the East Siberian and Beaufort Seas,

299   respectively. The implication is that the persistence of interannual variations about the trend line

makes only small contributions to interannual variations of pan-Arctic sea ice extent, and that these small contributions result mainly from the Pacific sector of the Arctic.

The lagged R^2 values relevant to predictions of the Barnett Severity Index are shown in Figure 9. Because the BSI is based primarily on ice conditions in the Beaufort Sea in August and September, it is not surprising that the correlation is largest for the Beaufort's ice extent in September, when the R^2 value is approximately 0.8 for data that are not detrended. The August and September values for the Chukchi are essentially as large as the corresponding Beaufort values, indicating a spatial coherence of the variations (with trends included) in the two regions. The antecedent extents in the East Siberian and Barents regions also explain significant fractions of the variance when the trends are included.

The blue bars in Figure 9 are the lagged R^2 values based on the detrended data. Because the trend's contribution to the predictability has been removed, these correlations provide the most meaningful assessment of the seasonal predictability if the BSI based on antecedent ice conditions. The largest correlations are for the Beaufort Sea, where the explained variances decrease from about 0.55 (R ~ 0.74) in September to about 0.10 (R ~ 0.32) in June. The correlations for the Chukchi are only slightly smaller, but the values for the East Siberian and Barents Seas are much smaller, generally below 0.10. Because the other regions showed no significant correlations based on the detrended data, we conclude that antecedent ice conditions in only the nearby seas enable predictions of detrended interannual variations of the BSI and only from about June onward. Moreover, that the skill at this seasonal lead time (a prediction made in June for September) accounts for only about 10% of the variance of the BSI.

5 Conclusion

The substantial decrease of Arctic sea ice over the past several decades is well documented (Cavalieri and Parkinson, 2012; Parkinson, 2014; Onarheim et al., 2018). Of all the regions considered here, only the Bering Sea does not show a negative trend (Onarheim et al., 2018, their Table 1). However, the extreme minima of Bering Sea ice during the past two winters (2016-17 and 2017-18) are starting to bring the Bering's trend into alignment with the other regions of the Arctic.

The prominence of the trends in the time series of regional as well as pan-Arctic ice extent makes it important to distinguish the contribution of the trend from other sources of predictability.

331   In this study we explored the use of several methods of detrending in order to evaluate the use of

332   ice anomaly persistence (autocorrelation) and regional cross-correlations as predictors of ice

333   variations. The two-piece linear trend evaluations generally have break-points (increases of

334   trends) in the 1990s, indicating that the rate of ice loss has been greater in the past two decades

335   than in the earlier portion of the satellite era that began in 1979.

336   Based on the raw (not detrended) time series, the antecedent ice extents provide significant

337   predictive skill for September pan-Arctic ice extent as well as for the Barnett Severity Index, which

338   is more specific to the Beaufort Sea. Significant portions of variance of both September metrics

339   are explained by the regional ice extents of prior seasons (and even years, given the multidecadal

340   scales of the trends). However, this predictive "skill" is attributable primarily to the trends in the

341   data. Removal of the trend leaves little forecast skill beyond a month or two when the forecast

342   method is limited to the relatively simple statistical correlations utilized here. The low skill for

343   the detrended September pan-Arctic ice extent is consistent with the findings of Stroeve et al.

344   (2014) based on the Sea Ice Outlook as part of the Study of Environmental Arctic Change

345   (SEARCH).

346   While there is statistical significance in the trend-derived skill at lead times of several seasons

347   and also in the remaining (detrended) skill at lead times of a month or two, statistical significance

348   does not equate to usefulness. Potential users of sea ice forecasts include local communities

349   engaging in offshore subsistence and travel activities, marine transport companies, offshore

350   resource extraction, and the tourism industry. The relatively small fractions of variance predictable

351   several months in advance using detrended data (Figures 6-9) will likely leave uncertainties that

352   are too great for many users. However the trend-derived skill, which can represent 50% or more

353   of the variance, may enable decisions if the interannual variations superimposed on the trend

354   represent acceptable risks for users of sea ice forecasts.

355   Challenges that follow from this study are (1) the placement of skill from other methods

356   (numerical models, heuristic approaches) into a framework of skill evaluation presented here, i.e.,

357   taking into account the skill attributable to trends, and (2) an assessment of the levels of skill

358   (reliability) necessary to enable decisions and planning by various user sectors. An avenue for

359   progress in both (1) and (2) is the Sea Ice Prediction Network, which is now entering its Phase 2

360   (https://www.arcus.org/sipn).

361

Acknowledgments

Funding for this work was provided by the Climate Program Office of the National Oceanic and
Atmospheric Administration through Grants NA16OAR4310162 and by the National Science
Foundation through Grant OPP-1749081. Florence Fetterer was supported by the CIRES/NOAA
Cooperative Agreement, NOAA Grant NA15OAR4320137.

368 **References**

369 Agnew, T. A., and Howell, S.: Comparison of digitized Canadian ice charts and passive microwave

370 sea-ice concentrations. Geoscience and Remote Sensing Symposium, 2002. IGARSS '02. 2002

371 IEEE International 1: 231- 233. doi: 10.1109/IGARSS.2002.1024996, 2002.

372 AMAP: Snow, Water, Ice and Permafrost in the Arctic: 2017 Update. Arctic Monitoring and

373 Assessment Programme, Oslo, Norway, xiv + 269 pp., 2017.

374 Barnett, D. G.: A long-range ice forecasting method for the north coast of Alaska. Sea Ice

375 Processes and Models, R. Pritchard, Ed., University of Washington Press, 402–409, 1980.

376 Blanchard-Wrigglesworth, E., Armour, K. C., and Bitz, C. M.: Persistence and inherent

377 predictability of Arctic sea ice in a GCM ensemble and observations. J. Climate, 24, 231-250,

378 2011.

379 Cavalieri, D. J., and Parkinson, C. L.: Arctic sea ice variability and trends, 1979-2010. Cryosphere,

380 6, 881-889, 2012.

381 Crowley Maritime Corporation, 2002. From

382 http://www.crowley.com/content/download/11926/80932/version/1/file/Alaska-50-Years.pdf

383 accessed 10 May 2018.

384 Drobot, S.: Long-range statistical forecasting of ice severity in the Baaufort-Chukchi Sea. Weather

385 and Forecasting, 18, 1161-1176, 2003.

386 Jones E., Oliphant, E. Peterson E. *et al.:* SciPy: Open Source Scientific Tools for Python, 2001-,

387 http://www.scipy.org/ [Online; accessed 2018-03-29].

388 Kinnard, C., Zdanowicz, C. M., Fisher, D. A., Isaksson, E., De Vernal, A., and Thompson, L. G.:

389 Reconstructed changes in Arctic sea ice over the past 1,450 years. Nature, 479, 509-512, 2011.

390 Kwok, R., and Rothrock, D. A.: Decline in Arctic sea ice thickness from submarine and ICESat

391 records: 1958-2008. Geophys. Res. Lett., 36, L15501, 2009.

392   Laxon, S.W., Giles, K. A.. Rideout, A. L., Wingham, D. J., Willatt, R., Cullen, R., Kwok, R.,

393   Schweiger, A., Zhang, J.,. Haas, C., Hendricks, S., Krishfield, R., Kurtz, N., Farrell, S., and

394   Davidson, M.: CryoSat-2 estimates of Arctic sea ice thickness and volume. Geophys. Res.

395   Lett., *40*, doi: 10.1002/grl.50193, 2013.

396   Lenton, T. M.: Arctic climate tipping points. Ambio, 41, 10-22, 2012.

397   Maslanik, J., Stroeve, J., Fowler, C., and Emery, W: Distribution and trends in Arctic sea ice age

398   through spring 2011. Geophys. Res. Lett., 38, L13502, doi:10.10029/2011GL047735, 2011.

399   Meier, W., Fetterer, F., Savoie, M., Mallory, S., Duerr, R., and Stroeve, J: NOAA/NSIDC Climate

400   Data Record of Passive Microwave Sea Ice Concentration, Version 2. Boulder, Colorado USA.

401   NSIDC: National Snow and Ice Data Center. doi:http://dx.doi.org/10.7265/N59P2ZTG.

402   (G02202), 2013.

403   National Ice Center and National Snow and Ice Data Center. Compiled by Fetterer, F., Savoie, M.,

404   Helfrich, S., and Clemente-Colón,: *Multisensor Analyzed Sea Ice Extent - Northern Hemisphere*

405   *(MASIE-NH), Version 1*. Boulder, Colorado USA. NSIDC: National Snow and Ice Data Center.

406   doi: https://doi.org/10.7265/N5GT5K3K, (G02186), 2010 (updated daily)

407   Onarheim, I. H., Eldevik, T., Smedsrud, L. H., and Stroeve, J. C.: Seasonal and regional

408   manifestations of Arctic sea ice. J. Climate, in press, doi:10.1175/JCLI-D-17-0427.1, 2018.

409   Parkinson, C. L.: Spatially mapped reductions in the length of the Arctic sea ice season. Geophys.

410   Res. Lett., 41, 4316-4322, 2014.

411   Partington, K., Flynn, T., Lamb, D., Bertoia, C., and Dedrick, K.: Late twentieth century Northern

412   Hemisphere sea-ice record from U.S. National Ice Center ice charts. J. Geophys. Res. 108(C11):

413   3343. doi:10.1029/2002JC001623, 2003.

414   Schweiger, A. J., Wood, K. R., and Zhang, J.: Arctic sea ice volume variability over 1901-2010:

415   A model-based reconstruction. J. Geophys. Res.-Oceans, in review, 2018.

416

417   Serreze, M. C., Stroeve, J., Barrett, A. P., and Boisvert, L. N.: Summer atmospheric circulation

418   anomalies over the Arctic Ocean and their influences on September sea ice extent: A cautionary

419   tale. J. Geophys. Res.-Atmospheres, 121(19): 11,463-11,485, doi:10.1002/2016JD025161, 2016.

420   Stroeve, J., Hamilton, L. C., Bitz, C. M., and Blanchard-Wrigglesworth, E.: Predicting September

421   sea ice: Ensemble skill of the SEARCH Sea Ice Outlook, 2008-2013. Geophys. Res. Lett., 41,

422   2411-2418, 2014.

423   Walsh, J. E., Fetterer, F., Stewart, J. S., and Chapman, W. L.: A database for depicting sea ice

424   variations back to 1850. Geograph. Rev., 107, 89-107, 2016.

425   Walsh, J. E., Chapman, W. L., and Fetterer, F.: Gridded Monthly Sea Ice Extent and

426   Concentration, 1850 Onward, Version 1. Boulder, Colorado USA. NSIDC: National Snow and

427   Ice Data Center. doi: http://dx.doi.org/10.7265/N5833PZ5, (G10010), 2015 (updated 2016).

Appendix. Reconstruction of the Barnett Severity Index, 1953-2013

As described in Section 2, the Barnett Severity Index (BSI) is a combination of five metrics of ice coverage in the Beaufort Sea. Drobot et al. (2003) used the BSI through 2000 in their evaluation of predictability based on multilinear regression against various measures of sea ice cover. In order to update the BSI for use in this study, we base a reconstruction on the digital grids of sea ice concentration in the Historical Sea Ice Atlas (HSIA) for Alaska (http://seaiceatlas.snap.uaf.edu/). As with the regional ice extent calculations using G10010 (Section 2), we use the HSIA because it extends the record 26 years back in time before the start of the satellite passive microwave record. While the sources of the ice concentration data in the HSIA are the same as in G10010, a notable advantage of the HSIA is its weekly temporal resolution (vs. the monthly resolution of G10010). The HSIA also has a spatial resolution of ¼° latitude by ¼° degree longitude. Because of the weekly time resolution, the distance metrics (3)-(5) of the BSI are truncated to the nearest week. Similarly, the distance metrics (1) and (2) are truncated to the nearest 27.8 km (15 n mi). One of the within-month dates of the HSIA grids is the 15th of each month, so no temporal interpolation is necessary for metrics (1) and (2). The reconstructed values of the BSI are listed in Table A1.

447

448
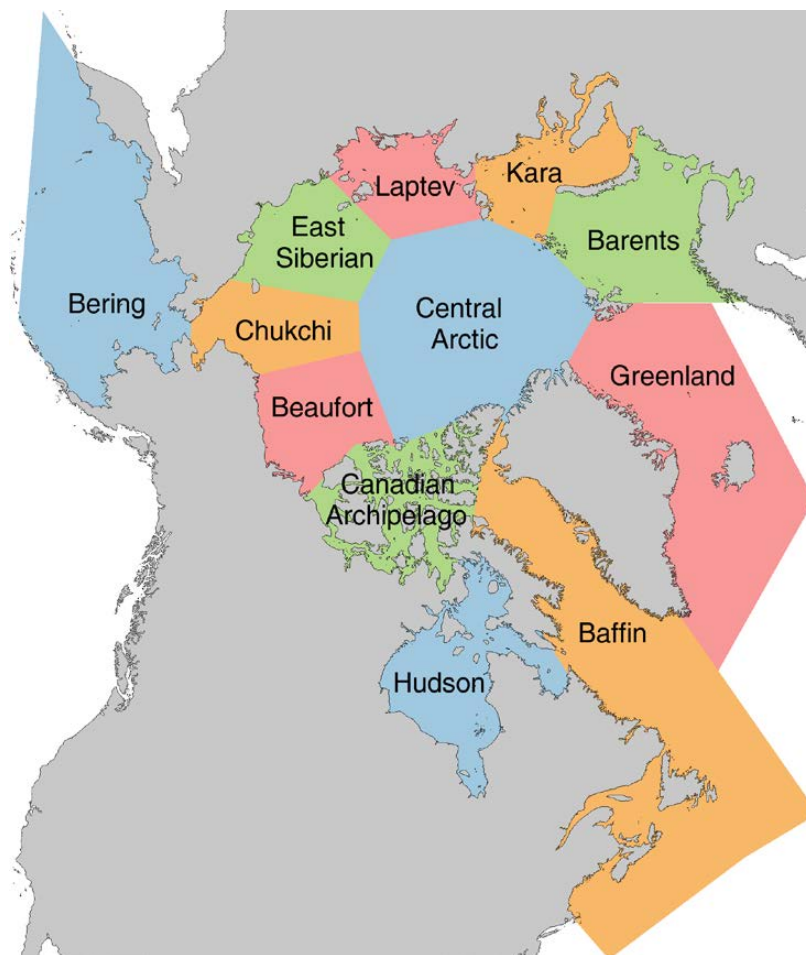
449   **Figure 1.** The MASIE subregions used in the study (NIC and NSIDC, 2010).

450

451
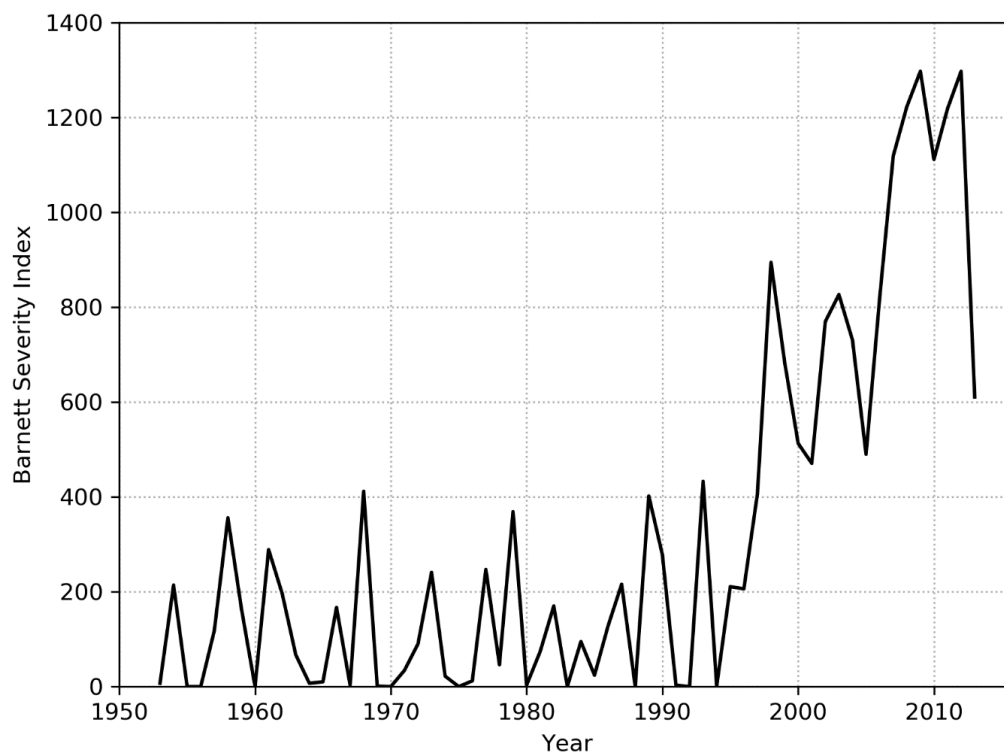
452   **Figure 2.** Time series of the Barnett Severity Index (BSI), 1953-2013.

453

454
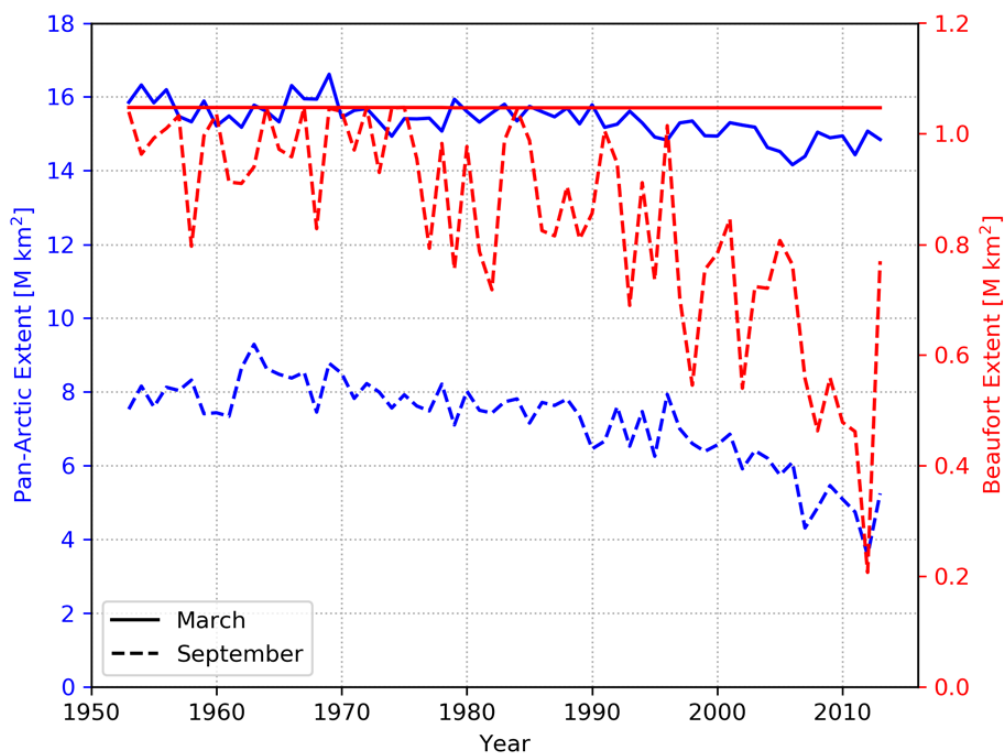
455

456 **Figure 3.** Total Arctic sea ice extent (blue) and the extent of ice in the Beaufort Sea (red) during

457   March and September.

458

459

460

461
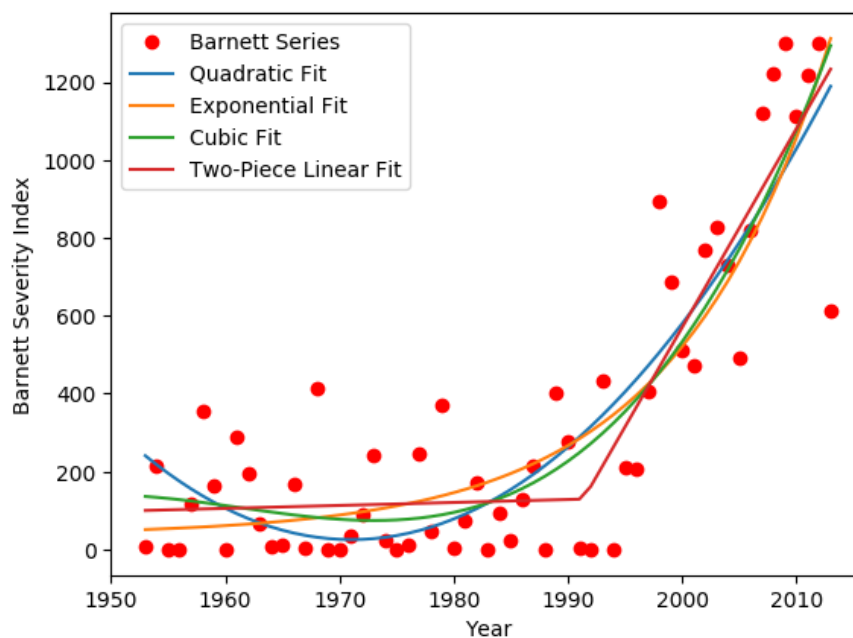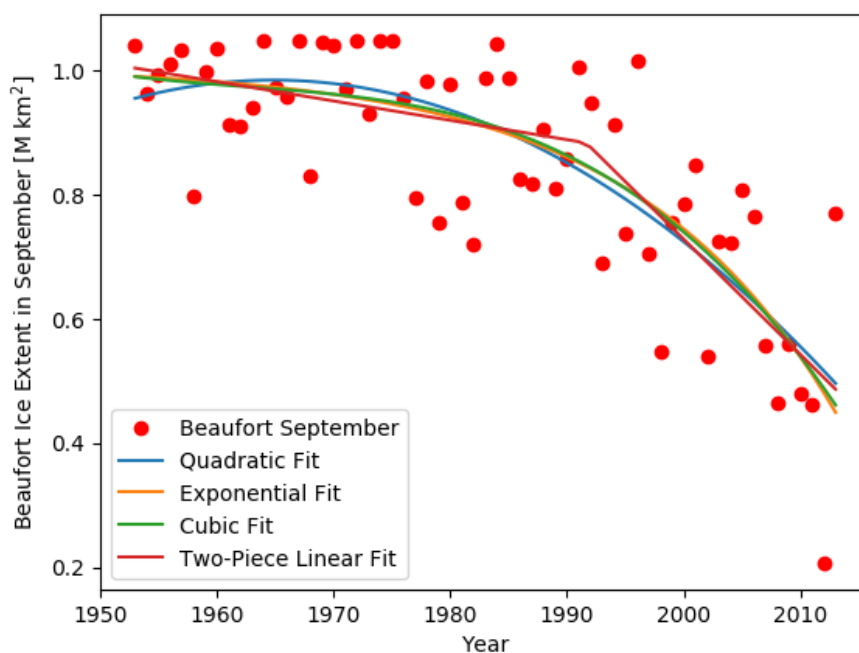
Figure 4. Examples of different fit methods (see legend) applied to the BSI (upper panel) and the
September Beaufort ice extent time series (lower panel).

464

465
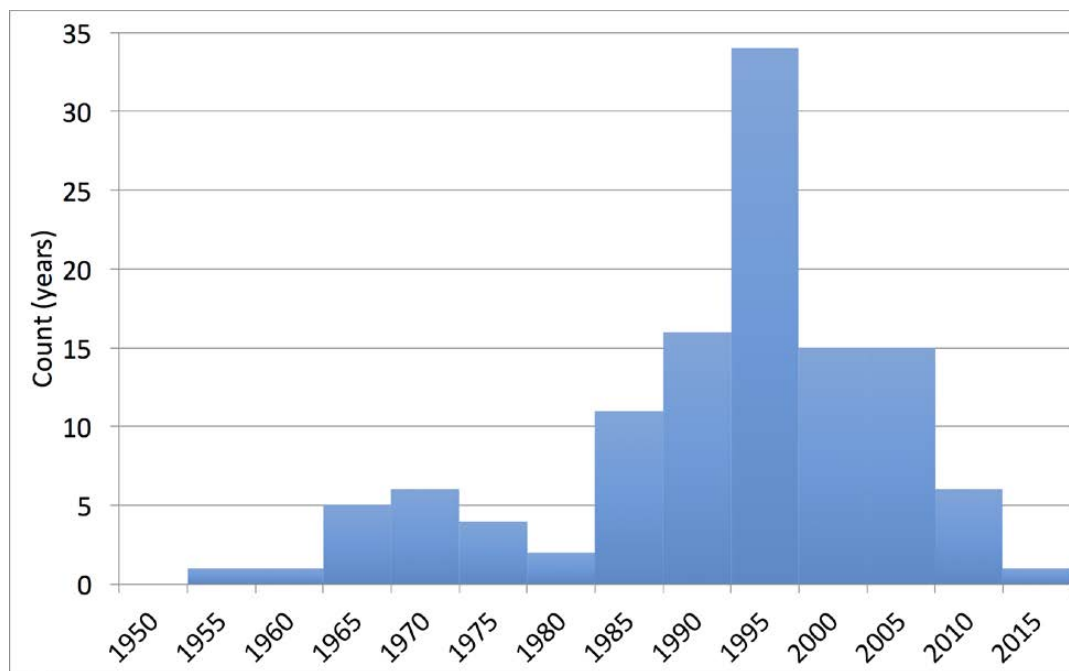
466

467

468   **Figure 5.** The distribution of break-point years across all regions and calendar months used in

469   the study. Years shown on the x-axis are ending years of 5-year periods.

470

471
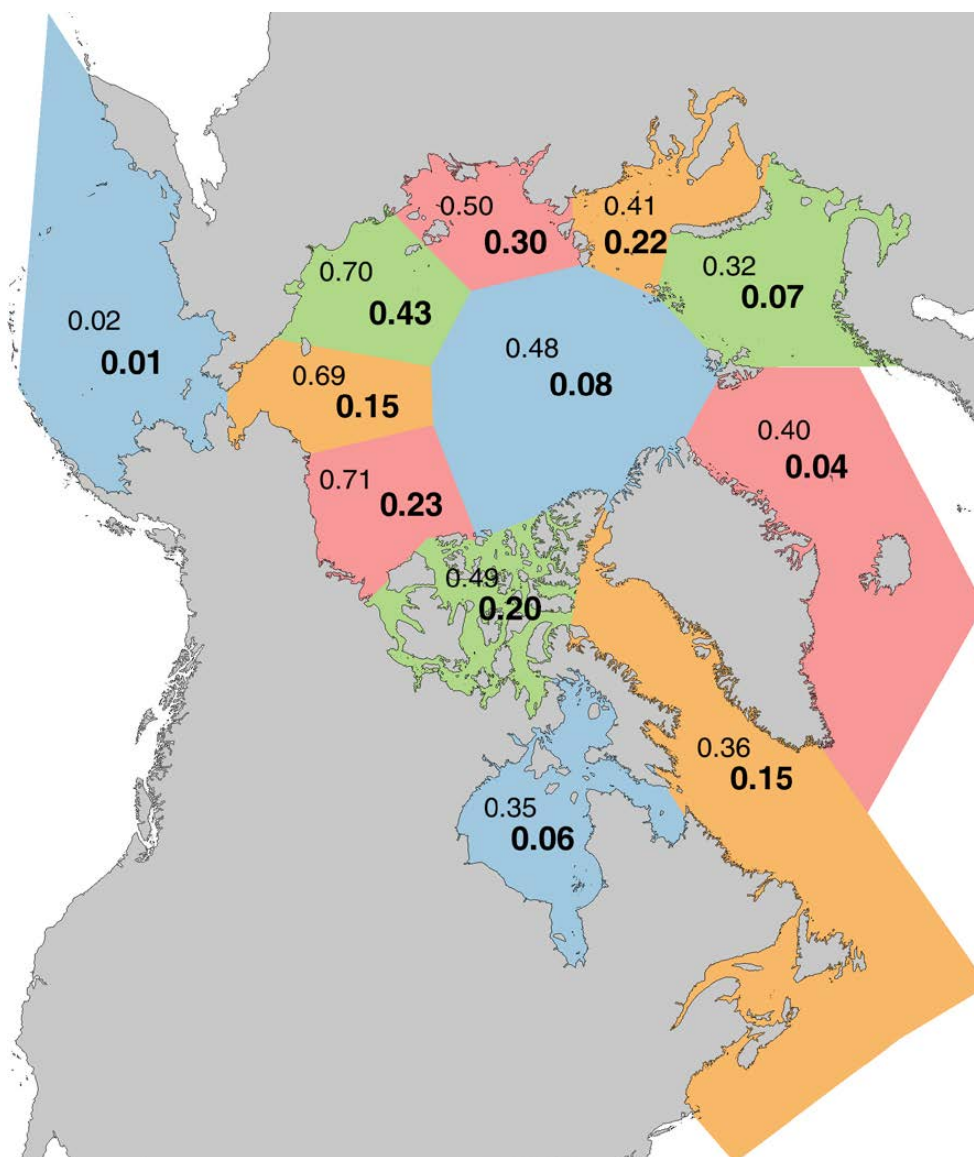
Figure 6. Squares of correlations (R^2) between September pan-Arctic ice extent and September regional ice extent based on ice extents including trends (upper numbers in normal font) and detrended (lower numbers, bold font).
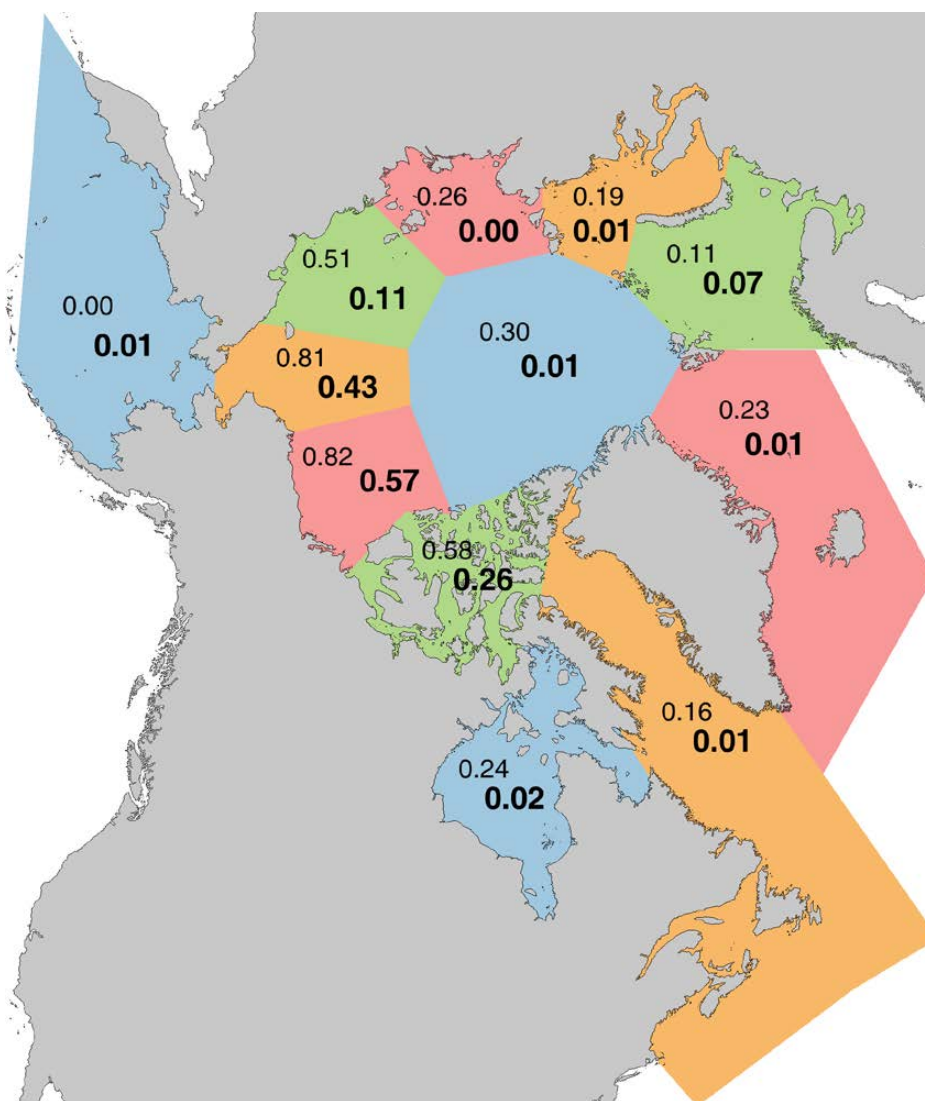
478
479
480   **Figure 7.** As in Figure 6, but for squares of correlations between the annual BSI and September
481   regional ice extents based on raw (not detrended) time series (upper numbers) and
482   detrended time series (lower numbers, bold font).
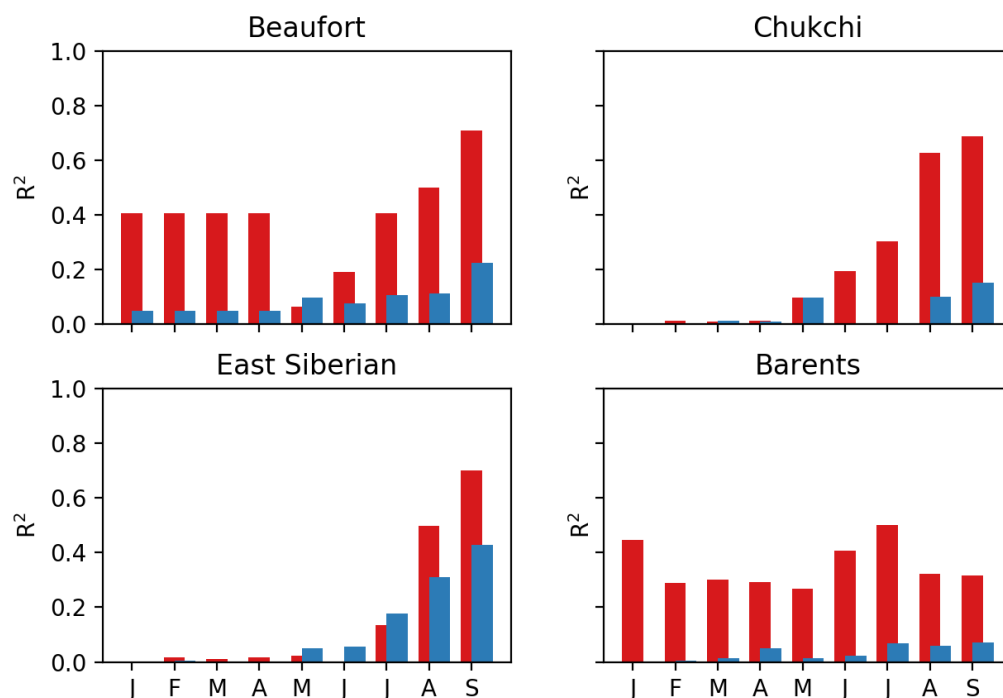
Figure 8. Examples of variances of September pan-Arctic ice extent and explained by correlations with antecedent regional ice extent in individual calendar months from September back to January (pan-Arctic extent lagging by 0, 1, 2, …, 8 months). Correlations are plotted as fractions of explained variance (squares of correlations). Red bars are correlations with trends included, blue bars are correlations after removal of trends.

490

491

492
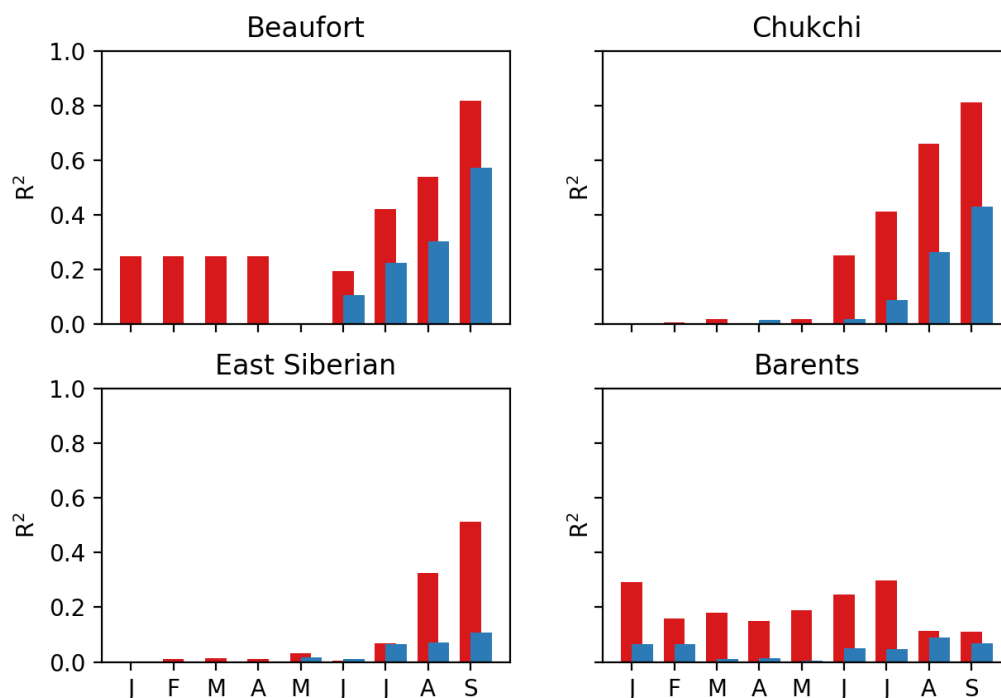
Figure 9. Examples of variances explained by correlations between the Barnett Severity Index
and regional ice extent in individual calendar months from September back to January
(BSI lagging by 0, 1, 2, …, 8 months). Correlations are plotted as fractions of explained
variance (squares of correlations). Red bars are correlations with trends included, blue
bars are correlations after removal of trends.

498

Region	Jan	Feb	Mar	Apr	May	Jun	Jul	Aug	Sep
Baffin-St. Lawrence	0.08	0.06	0.02	0.16	0.32	0.49	0.61	0.52	0.36
Barents	0.45	0.29	0.30	0.29	0.27	0.41	0.50	0.32	0.32
Beaufort	0.41	0.41	0.41	0.41	0.06	0.19	0.41	0.50	0.71
Bering	0.00	0.00	0.01	0.00	0.01	0.12	0.08	0.01	0.02
Canadian Archipelago	0.41	0.41	0.41	0.41	0.00	0.13	0.09	0.52	0.49
Central Arctic	0.21	0.11	0.18	0.01	0.02	0.02	0.15	0.07	0.48
Chukchi	0.00	0.01	0.01	0.01	0.10	0.20	0.31	0.63	0.69
East Siberian	0.00	0.02	0.01	0.02	0.02	0.00	0.14	0.50	0.70
Greenland	0.47	0.53	0.50	0.48	0.43	0.41	0.45	0.29	0.40
Hudson	0.05	0.41	0.41	0.26	0.03	0.32	0.66	0.37	0.35
Kara	0.00	0.03	0.11	0.04	0.10	0.09	0.44	0.42	0.41
Laptev	0.40	0.15	0.30	0.29	0.05	0.07	0.28	0.42	0.50
Pan-Arctic	0.50	0.44	0.40	0.50	0.48	0.64	0.84	0.91	1.00

Table 1. Correlations between monthly regional ice extent and pan-Arctic ice extent expressed as explained variance (R^2). Cases where 10% or more of the variance in pan-Arctic ice extent is explained by regional ice extent in a given antecedent month are highlighted with region names are bolded.

Region	Jan	Feb	Mar	Apr	May	Jun	Jul	Aug	Sep
Baffin-St. Lawrence	0.09	0.04	0.08	0.06	0.01	0.00	0.03	0.16	0.15
Barents	0.00	0.01	0.01	0.05	0.01	0.02	0.07	0.06	0.07
Beaufort	0.05	0.05	0.05	0.05	0.10	0.08	0.11	0.11	0.23
Bering	0.01	0.01	0.08	0.03	0.02	0.00	0.01	0.01	0.01
Canadian Archipelago	0.05	0.05	0.05	0.05	0.01	0.02	0.02	0.16	0.20
Central Arctic	0.02	0.02	0.11	0.03	0.02	0.04	0.07	0.00	0.08
Chukchi	0.00	0.00	0.01	0.01	0.10	0.00	0.00	0.10	0.15
East Siberian	0.00	0.00	0.00	0.00	0.05	0.06	0.18	0.31	0.43
Greenland	0.06	0.04	0.09	0.07	0.03	0.06	0.04	0.00	0.04
Hudson	0.00	0.05	0.05	0.01	0.05	0.01	0.11	0.07	0.06
Kara	0.01	0.03	0.03	0.04	0.00	0.18	0.12	0.13	0.22
Laptev	0.05	0.00	0.02	0.02	0.01	0.08	0.18	0.21	0.30
Pan-Arctic	0.03	0.02	0.00	0.00	0.01	0.04	0.24	0.70	1.00

Table 2. Correlations between detrended monthly regional ice extent and detrended September pan-Arctic ice extent expressed as explained variance (R^2). Cases where 10% or more of the variance in September pan-Arctic ice extent is predictable by regional ice extent in a given antecedent month are highlighted with region names are bolded.

512

Region	Jan	Feb	Mar	Apr	May	Jun	Jul	Aug	Sep
Baffin-St. Lawrence	0.20	0.14	0.07	0.23	0.31	0.44	0.49	0.30	0.16
Barents	0.29	0.16	0.18	0.15	0.19	0.25	0.30	0.11	0.11
Beaufort	0.25	0.25	0.25	0.25	0.00	0.19	0.42	0.54	0.82
Bering	0.00	0.00	0.03	0.02	0.04	0.10	0.11	0.01	0.00
Canadian Archipelago	0.25	0.25	0.25	0.25	0.03	0.13	0.13	0.49	0.58
Central Arctic	0.09	0.06	0.14	0.02	0.06	0.03	0.12	0.02	0.30
Chukchi	0.00	0.01	0.02	0.00	0.02	0.25	0.41	0.66	0.81
East Siberian	0.00	0.01	0.01	0.01	0.03	0.01	0.07	0.33	0.51
Greenland	0.26	0.31	0.34	0.32	0.27	0.23	0.28	0.17	0.23
Hudson	0.07	0.25	0.25	0.14	0.07	0.38	0.52	0.20	0.24
Kara	0.03	0.03	0.07	0.07	0.08	0.05	0.32	0.21	0.19
Laptev	0.25	0.11	0.18	0.20	0.05	0.03	0.16	0.22	0.26
Pan-Arctic	0.39	0.31	0.34	0.38	0.36	0.46	0.64	0.59	0.74

513

514

515 **Table 3.** The correlation between monthly regional ice extent and BSI expressed explained

516 variance (R^2). Cases where 10% or more of the variance in BSI is explained by regional ice extent

517 in a given antecedent month are highlighted with region names are bolded.

518

519

Region	Jan	Feb	Mar	Apr	May	Jun	Jul	Aug	Sep
Baffin-St. Lawrence	0.00	0.00	0.02	0.01	0.00	0.01	0.01	0.00	0.01
Barents	0.07	0.07	0.01	0.01	0.01	0.07	0.05	0.09	0.07
Beaufort	0.00	0.00	0.00	0.00	0.01	0.11	0.23	0.30	0.57
Bering	0.00	0.00	0.00	0.02	0.02	0.00	0.05	0.01	0.01
Canadian Archipelago	0.00	0.00	0.00	0.00	0.15	0.02	0.06	0.08	0.26
Central Arctic	0.08	0.13	0.09	0.01	0.00	0.02	0.17	0.09	0.01
Chukchi	0.00	0.00	0.01	0.02	0.00	0.02	0.09	0.26	0.43
East Siberian	0.00	0.00	0.00	0.00	0.02	0.01	0.07	0.07	0.11
Greenland	0.04	0.01	0.00	0.00	0.00	0.00	0.00	0.04	0.01
Hudson	0.01	0.00	0.00	0.01	0.00	0.01	0.03	0.00	0.02
Kara	0.08	0.04	0.00	0.01	0.00	0.02	0.00	0.04	0.01
Laptev	0.00	0.00	0.00	0.04	0.00	0.01	0.00	0.00	0.00

520

521

522 **Table 4.** The correlation between detrended monthly regional ice extent and detrended BSI

523 expressed as explained variance (R^2). Cases where 10% or more of the variance in BSI is explained

524 by regional ice extent in a given antecedent month are highlighted with region names are bolded.

Year	BSI	Year	BSI
1953	7	1984	95
1954	213	1985	24
1955	0	1986	178
1956	0	1987	216
1957	117	1988	0
1958	356	1989	402
1959	163	1990	278
1960	0	1991	3
1961	289	1992	0
1962	195	1993	434
1963	66	1994	1
1964	7	1995	211
1965	10	1996	206
1966	167	1997	407
1967	3	1998	895
1968	412	1999	685
1969	1	2000	513
1970	0	2001	471
1971	34	2002	770
1972	90	2003	827
1973	240	2004	731
1974	22	2005	490
1975	0	2006	819
1976	13	2007	1119
1977	247	2008	12239
1978	46	2009	12989
1979	368	2010	1112
1980	3	2011	1219
1981	74	2012	1298
1982	170	2013	611
1983	0		

Table A1. Yearly values of the Barnett Severity Index (BSI). Source: Rebecca Rolph, Geophysical Institute, University of Alaska, Fairbanks.